Population Effects on the Metallicity Distribution Function Derived From the Red Giant Branch

Antonio J. Ordoñez[1]
a.ordonez@ufl.edu
and

Ata Sarajedini[1]
ata@astro.ufl.edu

ABSTRACT

We have tested the reliability of the red giant branch (RGB) as a metallicity indicator accounting for observational errors as well as the complexity of star formation histories (SFHs) and chemical evolution histories observed in various stellar systems. We generate model color-magnitude diagrams (CMDs) produced with a variety of evolutionary histories and compare the resultant metallicity estimates from the colors and magnitudes of RGB stars to the true input metallicities. We include realistic models for photometric errors and completeness in our synthetic CMDs. As expected, for simple stellar populations dominated by old stars, the RGB provides a very accurate estimate of the modular metallicity value for a population. An error in the age of a system targeted for this type of study may produce metallicity errors of a few tenths of a dex. The size of this metallicity error depends linearly on the age error, and we find this dependence to be stronger with more precise photometry. If the population has experienced any significant star formation within the last ∼6 Gyr, the metallicity estimates, [M/H], derived from the RGB may be in error by up to ∼0.5 dex. Perhaps the most important consideration for this technique is an accurate, independent estimate of the average age for the target stellar system, especially if it is probable that a significant fraction of the population formed less than ∼6 Gyr ago.

Subject headings: stars: abundances - stars: HertzsprungRussell and CM diagrams - galaxies: dwarf - galaxies: stellar content - Local Group

1. Introduction

The red giant branch (RGB) phase in intermediate- to low-mass stellar evolution corresponds to the phase just before the onset of helium fusion. During the RGB phase, a star contains an electron degenerate core surrounded by a hydrogen-burning shell fueled by the CNO cycle (Chiosi 1998).

The color of the RGB on a color-magnitude diagram (CMD) strongly depends on the metal abundance of the stellar population (e.g. Da Costa & Armandroff (1990)). For this reason, the RGB has been widely used to obtain average metallicity estimates for a variety of stellar systems in the form of straightforward empirical calibrations between magnitude, color, and metallicity (Da Costa & Armandroff 1990; Saviane et al. 2000; Streich et al. 2014). However, the morphology and position of the RGB also depend somewhat on the age of the population, especially for stellar populations younger than ∼10 Gyr. Thus, given an estimate for the age of a stellar population, the metallicity distribution function (MDF) of the system can be calculated by comparing the RGB with theoretical isochrones of the appropriate age (Sarajedini & Jablonka 2005; McConnachie et al. 2006) or

[1]Department of Astronomy, University of Florida, 211 Bryant Space Science Center, Gainesville, FL 32611, USA

fiducial RGB sequences for discrete ages (Durrell, Harris, & Pritchet 2001).

Previously, Salaris & Girardi (2005) had investigated biases in determining the tip of the red giant branch (TRGB) based in the galaxies LMC, SMC, and LGS3 using synthetic CMDs. That study investigated some population effects on metallicities derived from the synthetic CMDs representing these systems. In this work, we provide a more thorough investigation of the degree to which star formation history can influence the results of these types MDF analyses mentioned above. To facilitate this, we generate model CMDs with a variety of star formation histories (SFHs) and chemical evolution histories and calculate the MDFs by interpolating amongst a grid of isochrones. In Section 2, we outline the methods used, detailing how the synthetic CMDs were created, how error and completeness profiles were applied, and how the interpolations were performed. Results are presented in Section 3, and we conclude our findings in Section 4.

2. Methods

2.1. Synthetic CMDs

To generate the synthetic CMDs, we utilize IAC-STAR[1] (Aparicio & Gallart 2004). This web browser-based software package generates synthetic CMDs through bilogarithmic interpolation in age and metallicity for a given set of stellar evolution libraries. IAC-STAR allows the user to enter unique SFHs and age-metallicity relations (AMRs) to synthesize arbitrarily complex stellar populations. It does so by taking as input up to 20 nodes in time with corresponding star formation rates (SFRs) and metallicities. The code then performs interpolations between these nodes to achieve satisfactory temporal resolution.

The stellar properties are calculated for each star and then converted to absolute magnitudes in a range of different filter sets with a variety of bolometric correction libraries. We utilize the stellar evolution library of Girardi et al. (2000) along with the bolometric correction library from Girardi et al. (2002). We chose this combination after our own exploration revealed that the RGBs produced from IAC-STAR with the stellar evolution library of Girardi et al. (2000) more closely matched the corresponding isochrones than the other stellar evolution libraries made available. We retrieved the isochrones to construct the interpolation grid using the CMD v2.1 web interface[2] since these utilize the same bolometric correction library used by IAC-STAR. For simplicity, we use a distance modulus of zero, zero reddening, a Kroupa IMF (Kroupa 2001), and an age of 13.5 Gyr for the universe in all of our models. We also set the mass-loss parameters for the RGB and AGB to $\eta = 0.2$ since we focus on old (low-mass) populations. As we are interested in magnitudes consistent with the brighter RGB ($-4 \lesssim \mathrm{M_I} \lesssim 0$) in the present study, we set the limit for output from IAC-STAR to $\mathrm{M_V} = 2$ mag.

2.2. Photometric Errors and Completeness

In order to realistically model the observational characteristics of CMDs, we follow the prescription of Barker, Sarajedini, & Harris (2004). In that work, they tested the reliability of the TRGB using synthetic CMDs where they modeled the photometric error and completeness profiles using simple analytic functions. Photometric errors for both $\mathrm{M_V}$ and $\mathrm{M_I}$ are modeled with an exponential function:

$$\sigma(\mathrm{M}) = \kappa e^{\tau \mathrm{M}} \tag{1}$$

where κ and τ are coefficients that describe the shape of the error profile. The completeness at a given magnitude is modeled as:

$$f(\mathrm{M}) = -\frac{2}{\pi} \arctan[\alpha(\mathrm{M} - \mathrm{M_0})] \tag{2}$$

where α is a shape parameter and $\mathrm{M_0}$ is the magnitude at which completeness falls to 0%.

In an effort to sample two extremes in error and completeness, we define two error and completeness profiles in the following way. For the first case, we utilize the same error and completeness profiles from Barker, Sarajedini, & Harris (2004), which will be denoted as observational profile A. The relevant coefficients for this error profile are listed in Table 1. This results in typical errors on the RGB of $\leq$0.05 mag at absolute magnitudes brighter than M = -2 mag and a completeness of

[1] http://iac-star.iac.es

[2] http://stev.oapd.inaf.it/cgi-bin/cmd_2.1

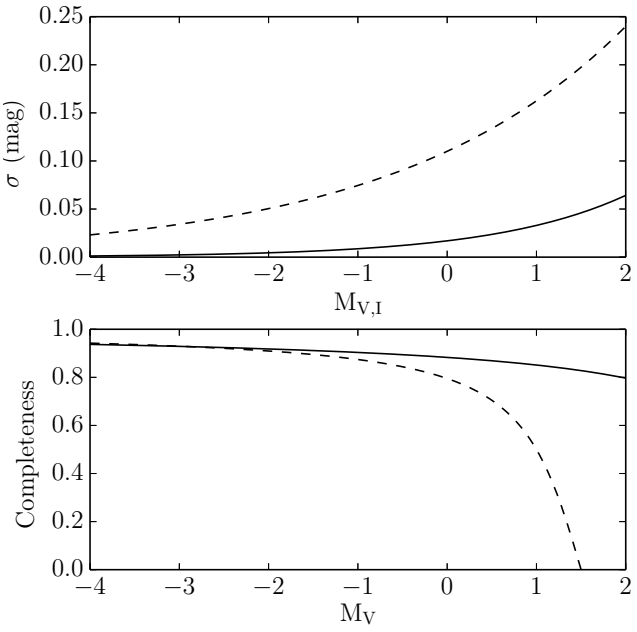

Fig. 1.— Both adopted error and completeness profiles. *Top:* Photometric error as a function of absolute magnitude, both in V and I. The dashed line corresponds to Profile A, while the solid line corresponds to Profile B. *Bottom:* Completeness as a function of M_V. Symbols are as for the top panel.

50% at $M_V = 1$ mag. A typical CMD obtained using this profile contains ∼2200 stars.

The second case is aimed at representing a less conservative error profile similar to *Hubble Space Telescope* (HST) imaging of a Local Group dwarf galaxy, which we will denote as observational profile B. In particular, we utilized the photometry from Hidalgo et al. (2009) using HST imaging of the dwarf transition-type galaxy, Phoenix, for which the data are deep enough to sample the RGB 6 magnitudes fainter than the TRGB. From the photometry provided by S. Hidalgo (private communication; 2013), we fit functions of the form shown in Equation (1) and (2) to the photometric errors and completeness. We note that Barker, Sarajedini, & Harris (2004) utilized the same error profile for both V and I, and we do the same here, as we found there to be little difference between them. We therefore use the fit from the I-band photometric errors. The coefficients for profile B are also listed in Table 1 for comparison. Typical errors on the RGB for Profile B are ∼0.01 mag. Both error and completeness profiles are plotted for comparison in Figure 1. Finally, in order to realistically simulate the density of stars on the CMD for a system like a dwarf galaxy, we scale each synthetic CMD such that the number of stars at $M_I = -3.0 \pm 0.1$ mag is ∼90. A typical CMD obtained using this profile contains ∼3500 stars brighter than $M_V = 2$ mag.

2.3. Metallicity Calculation

In an effort to derive metallicities from these synthetic CMDs in a manner similar to what has been done in past work, we chose to calculate the metallicity of each individual star on the RGB by interpolating among a grid of theoretical isochrones. Our procedure is modeled after that of Sarajedini & Jablonka (2005), and we utilize the same Interactive Data Language (IDL) code to perform the interpolations. To summarize the procedure, the isochrones represent a three-dimensional grid of M_I, $(V\text{-}I)_0$, and metal abundance for stars of a given age. The IDL routine *trigrid* then performs the interpolation for each star on the grid within a specified magnitude range. To estimate the errors in metallicity arising from the presence of photometric errors, we repeated the interpolation to account for photometric error in magnitude and color for each star, and the sum of

Table 1
Coefficients for different observational profiles.

Profile	κ	τ	α	M_0
A	0.11	0.39	2.0	1.0
B	0.02	0.67	1.18	4.57

these deviations in quadrature is assigned as the error in metallicity. We choose not to extrapolate beyond the grid since we found this to result in highly uncertain metallicities. Therefore, if any star falls off of the isochrone grid, either initially or after scattering to account for the photometric errors, we discard it from the final MDF.

Since the standard approach is to assume an old age for most systems to which this technique is applied, we use isochrones for an age of 12 Gyr as our fiducial grid. For systems older than ∼10 Gyr, the interpolated metallicities from RGB stars do not depend sensitively on the age of the isochrones used (Sarajedini & Jablonka 2005). Most previous work with this method tends to exclude stars fainter than some magnitude limit in order to remove contamination from stars on the horizontal branch (HB) and red clump (RC). We therefore limit our interpolations to magnitudes brighter than $M_I = -1.2$ mag. Finally, to obtain a singular estimate for the average metallicity, we construct a generalized histogram of the MDF (i.e. the Gaussian smoothed MDF using errors returned from the interpolation algorithm) and take the peak of this distribution as the representative metallicity. We found this to be more robust against skewing effects inherent in this method (see Section 3.1) than the mean or median. For our analysis, the peak of the input MDFs are calculated in a similar manner, with arbitrarily low errors assigned to construct the distribution. Confidence intervals are calculated using a standard bootstrapping technique, and the resulting reported errors correspond to 99% confidence intervals, or 3σ uncertainties.

3. Results

3.1. A Simple Stellar Population: P1

We first synthesized the CMD of a simple population with one age of 12 Gyr, one metallicity of $Z = 0.001$ ([M/H] = -1.28 dex), and no binaries, which we will refer to as P1. We apply both observational profiles to this synthetic CMD, to which we will refer to as models 1A and 1B (see Section 2.2 for a description of the observational profiles). The CMDs are plotted in Figure 2.

As was mentioned previously, studies that employ interpolation on an isochrone grid typically limit the interpolation to stars brighter than some magnitude limit to prevent contamination of RC and HB stars on the model grid. Since a significant fraction of the AGB occupies similar magnitudes as the bright RGB, these stars will generally provide some contamination if present within a stellar population. Additionally, fainter stars have larger photometric errors, so at some point including fainter stars in the RGB may only act to add noise to interpolated MDFs. To further investigate how these factors affect the resultant MDF, we ran a series of interpolations on these two CMDs each time changing the faint magnitude limit, $M_{I,f}$, above which the interpolation was performed. In this way, we tested what magnitude range yields the most accurate and precise metallicity estimate. We use isochrones for an age of 12 Gyr and metallicities of $Z = 0.0001$, $Z = 0.0003$, $Z = 0.0006$, $Z = 0.001$, $Z = 0.002$, $Z = 0.004$, and $Z = 0.008$. The results from this set of interpolations are presented in Table 2 where the peak metallicity and its difference from the input peak are presented for each case.

Overall, it is clear that the interpolations produce fairly accurate values for the peak metallicity, given that all are within 0.1 dex of the input values. We illustrate this further in Figure 3 where

TABLE 2
RESULTS FROM VARYING THE FAINT LIMIT FOR THE INTERPOLATION.

Model	$M_{I,f}$ (mag)	Peak [M/H][a] (dex)	Δ[M/H] (dex)
1A	-3.5	-1.25 ± 0.05	-0.03
1A	-3.0	-1.24 ± 0.06	-0.04
1A	-2.5	-1.23 ± 0.05	-0.05
1A	-2.0	-1.22 ± 0.06	-0.06
1A	-1.5	-1.21 ± 0.05	-0.07
1A	-1.2	-1.20 ± 0.05	-0.08
1B	-3.5	-1.29 ± 0.01	0.01
1B	-3.0	-1.29 ± 0.01	0.01
1B	-2.5	-1.29 ± 0.01	0.01
1B	-2.0	-1.29 ± 0.01	0.01
1B	-1.5	-1.29 ± 0.01	0.01
1B	-1.2	-1.29 ± 0.01	0.01

[a]These results correspond to a simple stellar population with age 12 Gyr and [M/H] = -1.28 dex.

[b]Quoted uncertainties represent bootstrapped 99% confidence intervals.

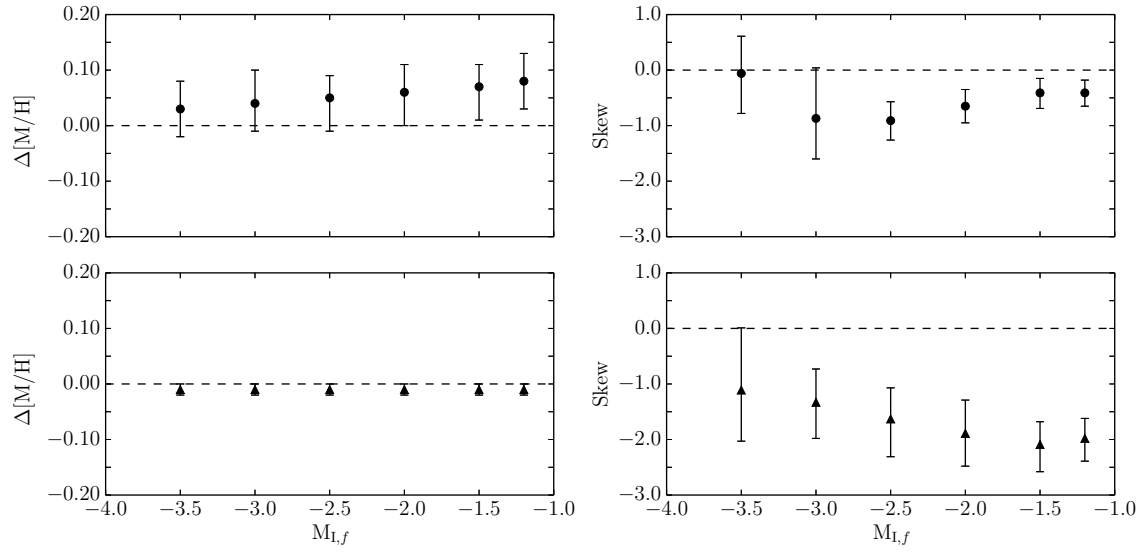

Fig. 3.— *Left:* Difference between peak metallicity estimates from isochrone interpolation and the input metallicity for Models 1A (circles) and 1B (triangles) as a function of the adopted threshold magnitude, $M_{I,f}$. *Right:* Skew of interpolated MDFs as a function of the adopted threshold magnitude, $M_{I,f}$. The dashed lines represent the input MDF values. *Top:* Interpolations for Model 1A. *Bottom:* Interpolations for Model 1B. The error bars represent 99% confidence intervals from a standard percentile bootstrap analysis.

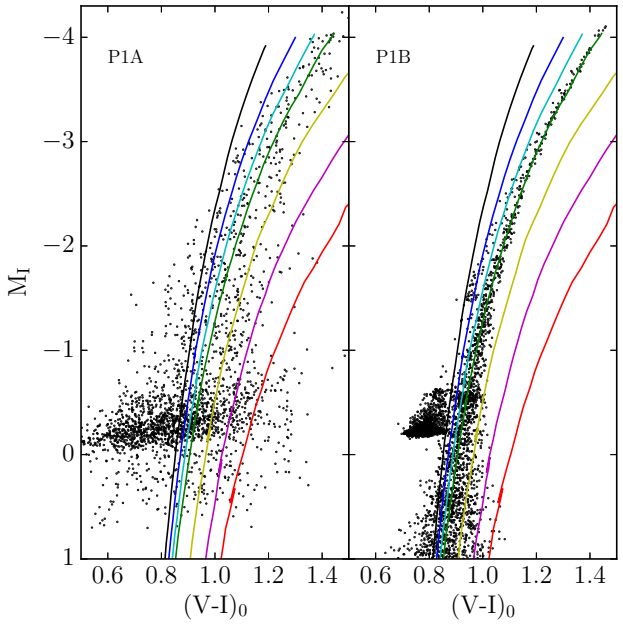

Fig. 2.— *Left:* The M_I, $(V-I)_0$ CMD for model 1A. The model grid using the isochrones of Girardi et al. (2002) for an age of 12 Gyr and metallicities of, from left to right, Z = 0.0001, 0.0003, 0.0006, 0.001, 0.002, 0.004, and 0.008 are overplotted for reference. Both the AGB and RC stars are strongly blended with the RGB due to the photometric errors. *Right:* The CMD for model 1B. In CMD 1B, both the AGB and RC are apparent as distinct from the RGB, although some of these stars still contaminate the model grid of isochrones.

we have plotted the difference between the input and output peak metallicities against $M_{I,f}$.

For model 1B, the interpolation proves very reliable owing to the smaller photometric errors (3; bottom left), yielding peak metallicities which are both accurate and precise to within 0.01 dex. It seems that no matter where the interpolation is limited, the peak metallicities in the case of the small error profile yield systematically lower metallicities. The skew of this MDF, also illustrated in Figure 3, is consistent with skewness towards metal-poor values.

While this systematic offset in metallicity is within the errors, we note that one possible reason for systematically metal-poor values could be the AGB stars contaminating the grid at all magnitudes. Another possibility is that the asymmetric nature of the isochrone grid in the magnitude-color plane (i.e. the nonlinear dependence of the color of the RGB on [M/H]) produces this negative skew. Since the grid is asymmetric but the photometric errors are applied symmetrically, it follows that this effect could lead to some amount of artificial skewing. In order to further investigate these effects, we repeated the interpolations on P1 with the same observational profiles applied, however this time we excluded AGB stars from the final CMDs. This was achieved by applying cuts in initial mass, magnitude, and color such that stars more evolved than stars at the TRGB were filtered out. Note that the cuts in magnitude and color were only required due to the small but nonzero range in the ages of the stars in this simple stellar population resulting from the interpolation in time of the SFR by IAC-STAR. We then performed the interpolation down to magnitudes of $M_{I,f}$ = -1.2 mag. The resulting MDFs did not show any significant differences in peak metallicity or skew, forcing us to conclude that the AGB does not provide a significant source of contamination for an old, simple stellar population. Consequently, the asymmetry of the isochrone grid remains the only valid explanation, and we conclude that this asymmetry does provide a significant source of artificial negative skew to an interpolated MDF.

On the other hand, the model 1A yields systematically more *metal-rich* peaks than the input (Figure 3; top left). Additionally, this discrepancy grows as more faint RGB stars are included in the interpolation. While these differences are mostly

within the errors, its systematic nature could be of concern. We attribute this behavior to the interplay between the photometric errors and the isochrone grid. More specifically, the error profile for model 1A is such that a significant number of stars are observed off of the isochrone grid. This effect becomes more prominent for fainter stars since they have larger photometric errors, and the effect is asymmetric with respect to color. That is to say, the grid extends further in the redward direction than in the blueward direction. Thus, even though stars are scattered symmetrically in color due to the photometric errors, a greater number of stars will 'fall off' the model grid at the blue end. Simultaneously, stars that are scattered to redder colors are more likely to stay on the grid. This appears to diminish the skew of the MDF and move the peak to more metal-rich values. Once again, the skewness for model 1A (Figure 3; top right) seem to corroborate this behavior. The interpolated MDFs of model 1A appear systematically less skewed than those of model 1B.

Considering these effects, we now turn to determining the optimal cutoff for a metallicity interpolation on the RGB. Since we have determined AGB contamination to be negligible in an old stellar population, the fundamental competition governing the magnitude cutoff is between Poisson statistics and photometric errors. On the one hand, excluding more stars at fainter magnitudes reduces the number of stars in the sample, potentially leading to a metallicity estimate based on a prohibitively small sample of stars. On the other hand, including stars at fainter magnitudes allows stars with increasingly uncertain photometry, and thus metallicity, into the sample. This may lead, for example, to the peak metallicity discrepancy observed for model 1A. Thus, it seems that when the size of the photometric errors becomes comparable to the extent of the isochrone grid, interpolated metallicities may be subject to systematic errors.

To compromise between these two competing effects, we examined how the number of stars in the interpolation sample changed with $M_{I,f}$. Moving the limit from $M_{I,f}$ = -1.2 mag to $M_{I,f}$ = -1.5 mag results in losses of $\sim$14% (1A) and $\sim$20% (1B) of the stars above M_I = -1.2 mag (note the difference in fractional losses is due to the completeness profiles). Additionally, the interpolated MDFs are nearly identical in each case, with the only exception being a more accurate value for the peak metallicity in model 1A (Figure 3; top left). Making the cutoff brighter at $M_{I,f}$ = -2.0 mag resulted in losses of 40-50% of the stars above M_I = -1.2 mag with no significant increase in the accuracy of the interpolated metallicities. Under these considerations, we choose $M_{I,f}$ = -1.5 mag as our optimal cutoff and limit all future interpolations to stars brighter than this magnitude.

An anonymous referee suggested an alternative method to derive the peak metallicity of a population by constructing a fiducial RGB sequence from the photometry of the observed RGB. To accomplish this, we binned all of the stars brighter than the optimal cutoff, $M_{I,f}$ = -1.5 mag, into bins of 0.1 mag and then calculated the median $(V-I)_0$ color within each bin. The subsequent color paired with the midpoint of each magnitude bin served as our fiducial RGB which was input into the metallicity interpolation routine. We applied this method to both models 1A and 1B, and and the resulting differences between the input and output peaks in each case was 0.03 dex for model 1A and 0.01 dex for 1B. Comparing these Δ[M/H] with those listed in Table 2, it appears that this alternative method works well and recovers similarly accurate peaks. However, since this method removes information about the shape of the MDF, we shall continue to use the original, star by star interpolation to construct MDFs for the remainder of the paper.

Finally, we investigated how the metallicity of the simple stellar population affected the resulting metallicity interpolation. To this end, we synthesized a population whose properties were identical to P1, but having a metallicity of $Z = 0.0076$ ([M/H] = -0.4 dex). We performed the interpolation on the same grid in a similar manner to P1, and the errors in the peak metallicity amounted to $\sim$0.03 dex in [M/H]. Therefore, we conclude that the results of this interpolation method to be relatively insensitive to the bulk metallicity of the stellar population.

We conclude this section with some summarizing remarks. For an old, simple stellar population, isochrone interpolation on the RGB works very well to retrieve the peak metal abundance, with metallicity errors less than 0.1 dex for the worst case. In cases where the photometric errors are

large with respect to the size of the isochrone grid, exemplified in model 1A, the interpolated MDF and therefore peak metallicity are sensitive to the shape of the isochrone grid. For cases where the errors are small with respect to the model grid (1B), the MDF and its peak are accurately recovered to within 0.01 dex. We determine the best compromise between Poisson errors and photometric errors of an interpolated MDF to be to limit the interpolation to stars brighter than M_I=-1.5 mag. Finally, we conclude that this method is insensitive to the bulk metallicity of the population.

3.2. The Effects of a Metallicity Spread: P2

The limit of a simple stellar population with one age and one metallicity (i.e. [Fe/H]) is approximately valid for systems such as globular clusters (the effects of multiple populations and enhancement differences in individual globular clusters is beyond the scope of this work). However more complex systems, such as dwarf galaxies, require a more complex treatment. In particular, these systems typically show extended SFHs resulting in significant chemical evolution over time. Additionally, inherent metal abundance variations within a stellar population will also affect a metallicity determination. As a simple exploration of the effects of a metallicity spread, we created a synthetic CMD whose properties are identical to P1 (Section 3.1), with the only difference being a spread in the stellar metallicities. To accomplish this, we utilize a feature of IAC-STAR which allows the user to provide an upper and lower bound for the input AMR. IAC-STAR then calculates the metallicity of a star formed at any instant in time by randomly sampling a Gaussian bounded by these two AMRs at that time.

In this case, we set the lower AMR to a metallicity of $Z = 0.0006$ ([M/H] = -1.51 dex) and the upper AMR to a metallicity of $Z = 0.002$ ([M/H] = -0.98 dex), each constant in time, and we will henceforth refer to this as P2. The resulting input MDF is characterized by a mean metallicity of [M/H] = -1.20±0.15 dex, where the spread is calculated as one standard deviation. As with P1, we apply both observational profiles to this population and refer to these two CMDs as models 2A and 2B. We then performed the metallicity interpolation using the same grid from Section 3.1. The resulting model CMDs and MDFs are plotted together in Figure 4.

The peak interpolated metallicities for these model CMDs are [M/H] = $-1.10^{+0.06}_{-0.06}$ dex for 2A and [M/H] = $-1.07^{+0.15}_{-0.07}$ dex for 2B, and they differ from their input peaks by 0 dex and -0.04 dex respectively. Thus, each peak is again recovered well within the errors. Interestingly, model 2A has its peak recovered more accurately than model 2B. Although the discrepancy is within the errors, it is interesting to note that the skewness of MDF 2B is significantly more negative than for its input MDF. This is not true for MDF 2A. Similar behavior is observed for the simple stellar population in Section 3.1 (Figure 3; right column). Since the only difference between the two model CMDs is the observational profile applied, it seems that the photometric errors must be responsible for this. We interpret this to be related to the phenomenon previously observed and discussed in Section 3.1, namely the interaction of the photometric errors with the isochrone grid. Thus, even though MDF 2A suffers from more noise resultant from the larger photometric errors, it is less negatively skewed than MDF 2B because more stars are scattered off of the blue, metal-poor end of the grid than the red, metal-rich end. We emphasize that this systematic effect results in recovered peak metallicity for MDF 2A lying near the center of the isochrone grid and is not a reflection of higher accuracy. This illustrates the importance of ensuring that the photometric errors in a CMD upon which metallicity interpolation will be applied are small in comparison to the extent of the isochrone grid. In this case however, this effect is small.

To add to this, the error in the peak for 2A is significantly smaller than for 2B, even though the former suffers from larger photometric errors than the latter. To investigate the cause of this, we examined the bootstrapped distributions of the MDF peak for both model CMDs. This revealed a multimodal distribution of peak metallicities for MDF 2B. Specifically, in addition to the true peak at [M/H] = -1.07 dex, there also exist less prominent but still significant peaks at [M/H]∼-1.22 dex and [M/H]∼-1.03 dex. Careful examination of the generalized histogram of MDF 2B (Figure 4; bottom right) reveals these secondary peaks. These secondary peaks act to add uncertainty to the pri-

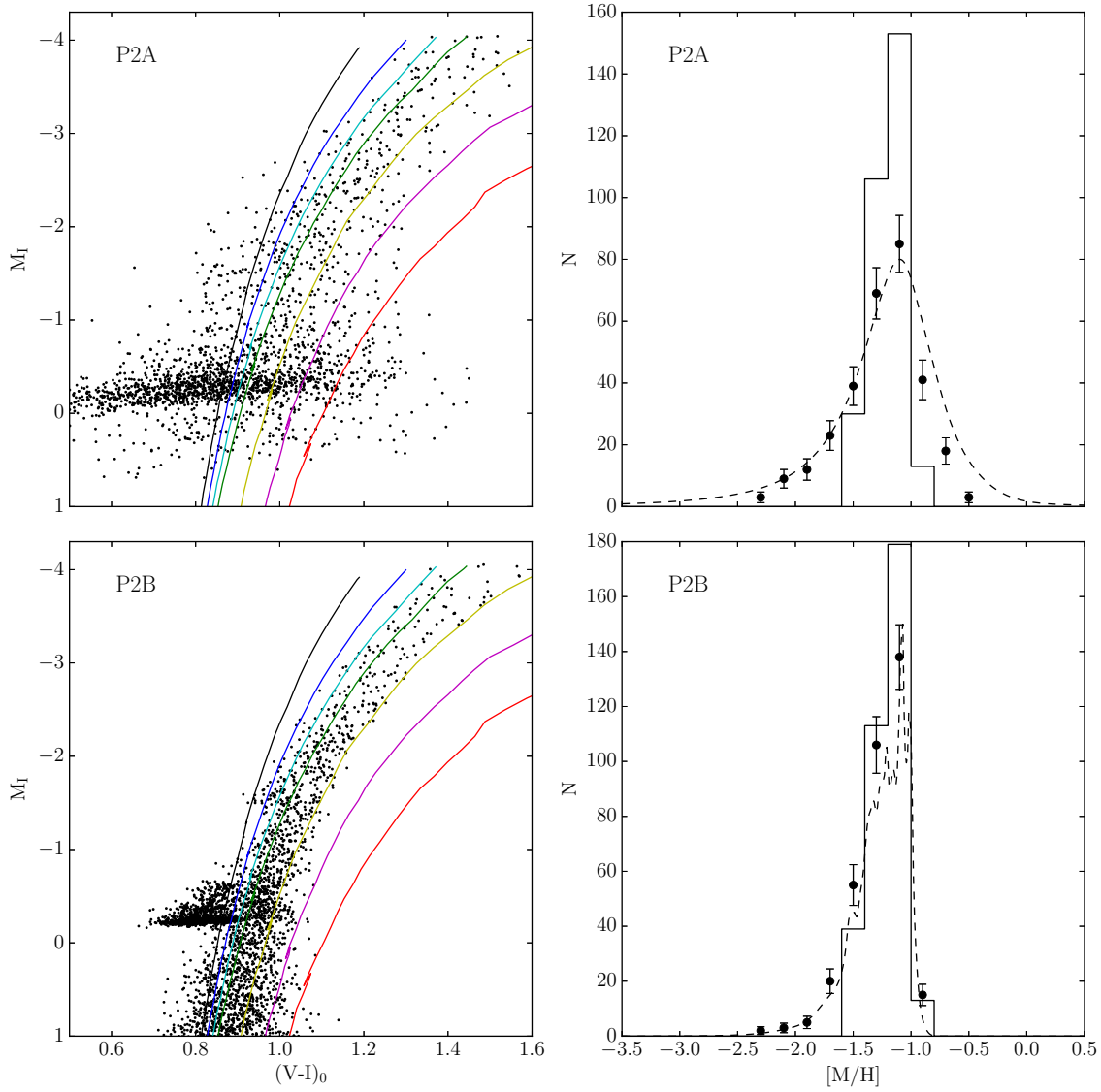

Fig. 4.— *Left:* The M_I, $(V\text{-}I)_0$ CMD for models 2A (*top*) and 2B (*bottom*). The model grid using the isochrones of Girardi et al. (2002) for an age of 12 Gyr and metallicities of $Z = 0.0001$, 0.0003, 0.0006, 0.001, 0.002, 0.004, and 0.008 are overplotted for reference.*Right:* The interpolated binned (points) and Gaussian smoothed (dashed line) MDFs for each corresponding model CMD. The error bars in the binned MDFs are 1σ Poisson uncertainties. The solid bar plots represent the input MDFs.

mary peak via our bootstrapping technique. It is therefore likely that we are over-estimating the errors in this case by using the 3σ errors. On the other hand, the larger photometric errors in CMD 2A smear these peaks out beyond recognition such that they do not present themselves in the bootstrapped distribution of the MDF peak. Taking into consideration all of the effects discussed in this subsection, we conclude that the peak interpolated metallicity is relatively insensitive to the effects of an inherent metallicity spread of order $\sigma \sim 0.15$ dex.

We conclude this subsection by noting that overall, the shape of the interpolated MDF 2B (4; bottom left, points) closely matches that of the input MDF (4; bottom left, solid line). The same is not true for MDF 2A (4). We note that the input MDFs for the two model CMDs differ slightly due to Poisson statistical effects introduced during the application of the completeness profile.

3.3. The Effects of an Age Spread: P3

We now turn to exploring the effects of a spread in the stellar ages. For this we synthesized a synthetic CMD whose properties are similar to the simple stellar population, P1, but whose SFH consists of a Gaussian with a mean age of 12 Gyr and a 1σ width of 2 Gyr. We designate this population as P3, and again apply the two observational profiles creating two models CMDs 3A and 3B. We performed the interpolation as before, and the results are illustrated in Figure 5.

The peak interpolated metallicities in this case are [M/H] = -1.20$^{+0.04}_{-0.05}$ dex for 3A and [M/H] = -1.30$^{+0.04}_{-0.02}$ dex for 3B. We note that these results are similar to that for the simple stellar population P1 (see Section 3.1). That is, the peak metallicity is well-recovered in the case of smaller photometric errors, albeit slightly metal-poor. The only effect of the age spread in this case is to increase the scatter from $\sim$0.01 dex to a few hundredths of a dex. On the other hand, the peak for 3A with its larger photometric errors is again more *metal-rich* than the input metallicity. This seems to be the result of the interplay of the photometric errors with the isochrone grid. In this case, the uncertainty in the peak remains the same as for a simple stellar population, indicating that the photometric errors wash out any signal of the age spread in this case. We therefore conclude that for an old age, the effects of an age spread of order $\sigma \sim 2$ Gyr do little to affect a metallicity interpolation. The peak is recovered with similar accuracy to a single-age population. The only observed effect is an increase in the error of the peak for the small error case, resulting in uncertainties still well below 0.1 dex in both cases.

3.4. The Effects of an Age and Metallicity spread: P4

We now add complexity to the synthetic CMD by inputting spreads in both metallicity and age. For this case, we essentially combine the AMR from P2 and the SFH from P3 and create an old population with mean age 12 Gyr, age spread of 2 Gyr, mean metallicity of [M/H]= -1.20 dex, and metallicity spread of 0.15 dex. This population is designated P4, and applying the observational profiles as before we have two model CMDs 4A and 4B. Performing the interpolations in the same way as with the previous models, we construct the MDFs along with their corresponding CMDs in Figure 6.

The peak interpolated metallicities for models 4A and 4B are [M/H] = -1.04$^{+0.08}_{-0.06}$ dex and [M/H] = -1.07$^{+0.19}_{-0.05}$ dex respectively. The peaks for both input MDFs are near [M/H] = -1.00 dex, so both peaks are recovered within their respective confidence intervals. One may note that the quoted uncertainties for these values are similar to those of models 2A and 2B, indicating that the metallicity spread dominates over the age spread in this case. Again, here it appears that we may be overestimating the errors in the case with the smaller photometric errors. The same mechanism discussed for model 2B in Section 3.2 seems to be at work for model 4B, namely the asymmetry of the isochrones in the CMDs and how this affects the metallicity interpolation. Aside from this, the peak metallicities are well-recovered in this case with both an age and metallicity spread.

3.5. The Effects of an Age Error

In the absence of an independent measure of the age of a stellar system, it is also interesting to investigate how a systematic error in the assumed age will affect a metallicity determination using the RGB. As was discussed above, for an

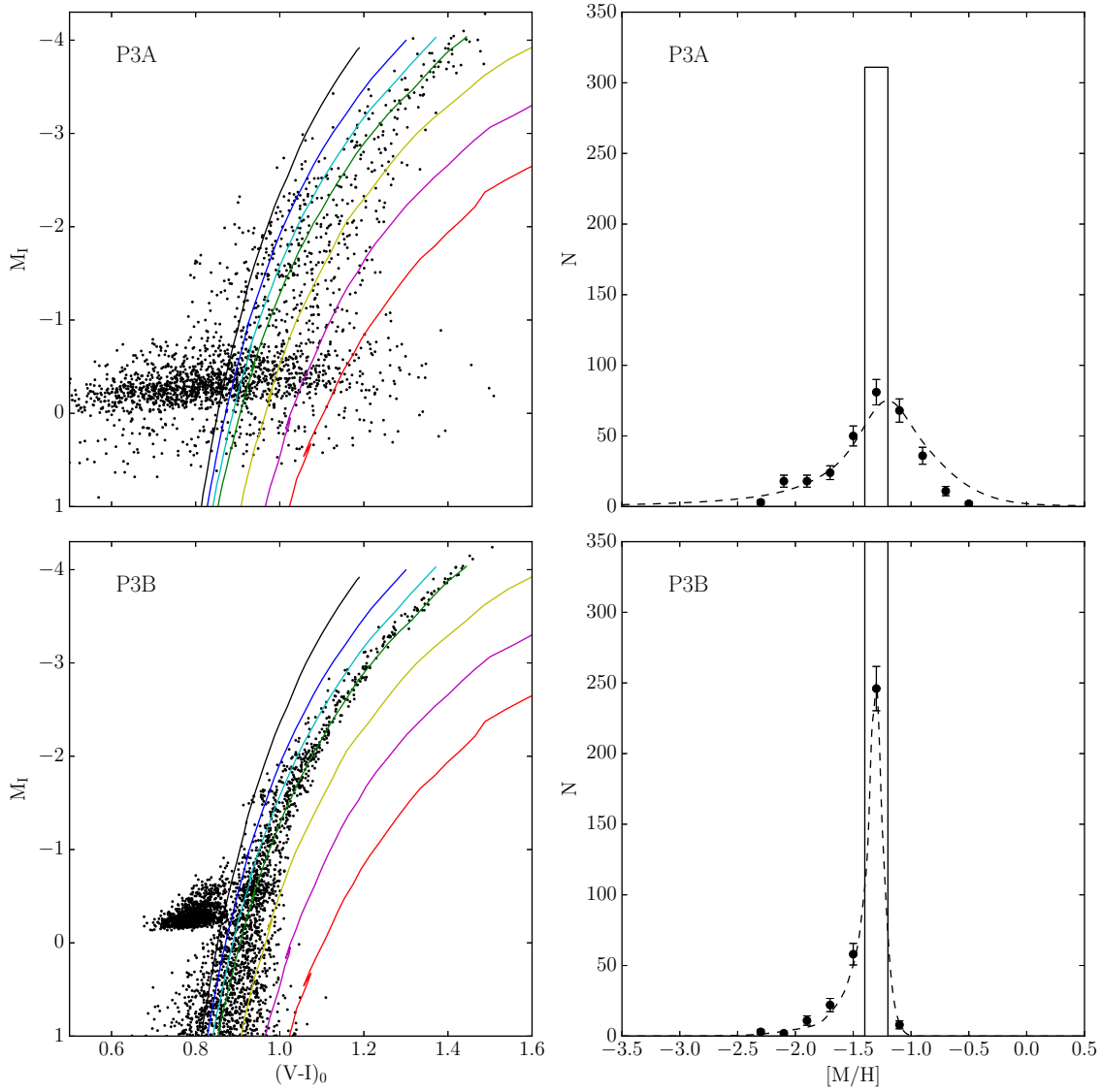

Fig. 5.— *Left:* The M_I, $(V\text{-}I)_0$ CMD for models 3A (*top*) and 3B (*bottom*). The model grid using the isochrones of Girardi et al. (2002) for an age of 12 Gyr and metallicities of $Z = 0.0001$, 0.0003, 0.0006, 0.001, 0.002, 0.004, and 0.008 are overplotted for reference.*Right:* The interpolated binned (points) and Gaussian smoothed (dashed line) MDFs for each corresponding model CMD. The error bars in the binned MDFs are 1σ Poisson uncertainties. The solid bar plots represent the input MDFs.

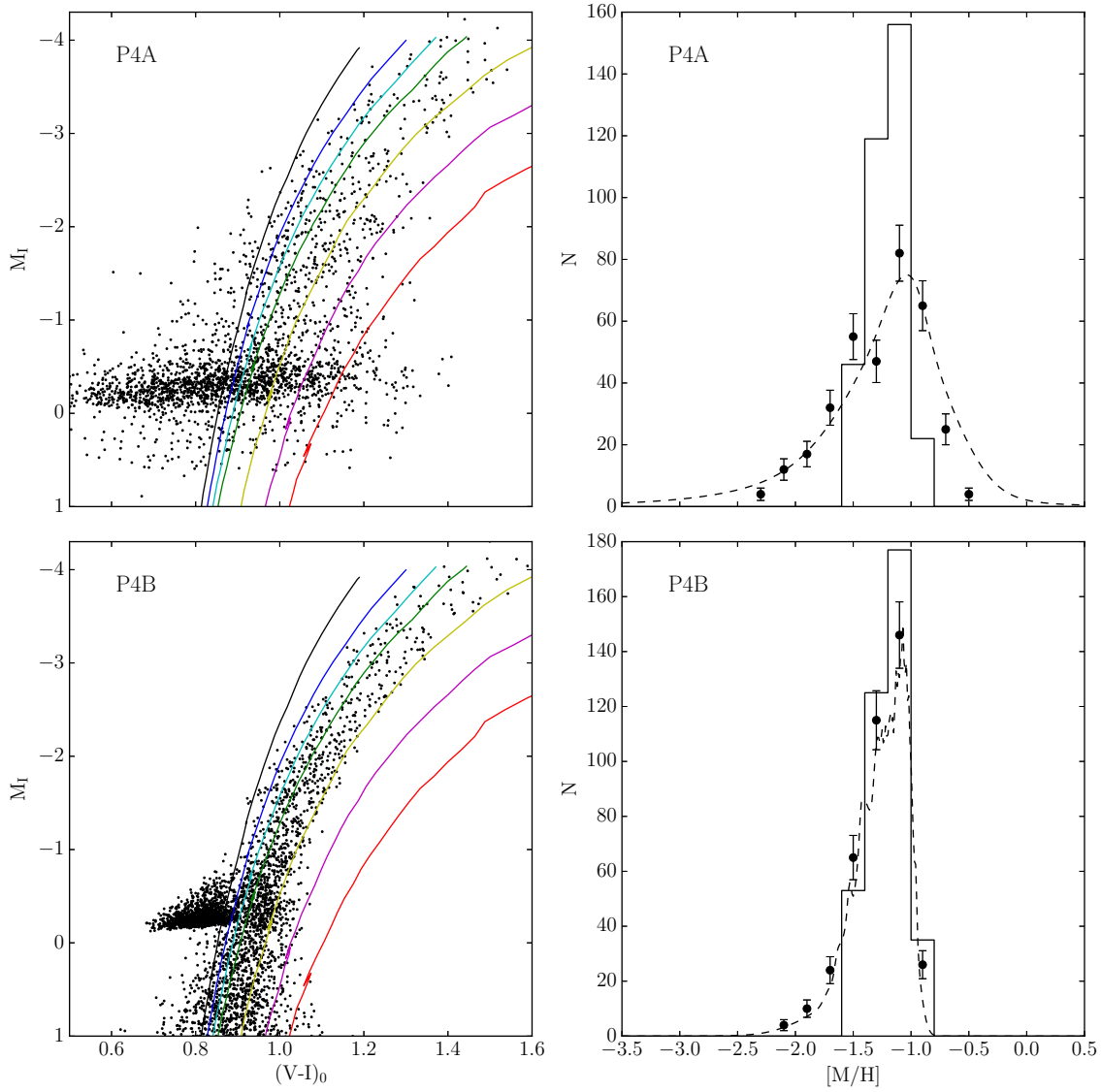

Fig. 6.— *Left:* The M_I, $(V\text{-}I)_0$ CMD for models 4A (*top*) and 4B (*bottom*). The model grid using the isochrones of Girardi et al. (2002) for an age of 12 Gyr and metallicities of $Z = 0.0001$, 0.0003, 0.0006, 0.001, 0.002, 0.004, and 0.008 are overplotted for reference.*Right:* The interpolated binned (points) and Gaussian smoothed (dashed line) MDFs for each corresponding model CMD. The error bars in the binned MDFs are 1σ Poisson uncertainties. The solid bar plots represent the input MDFs.

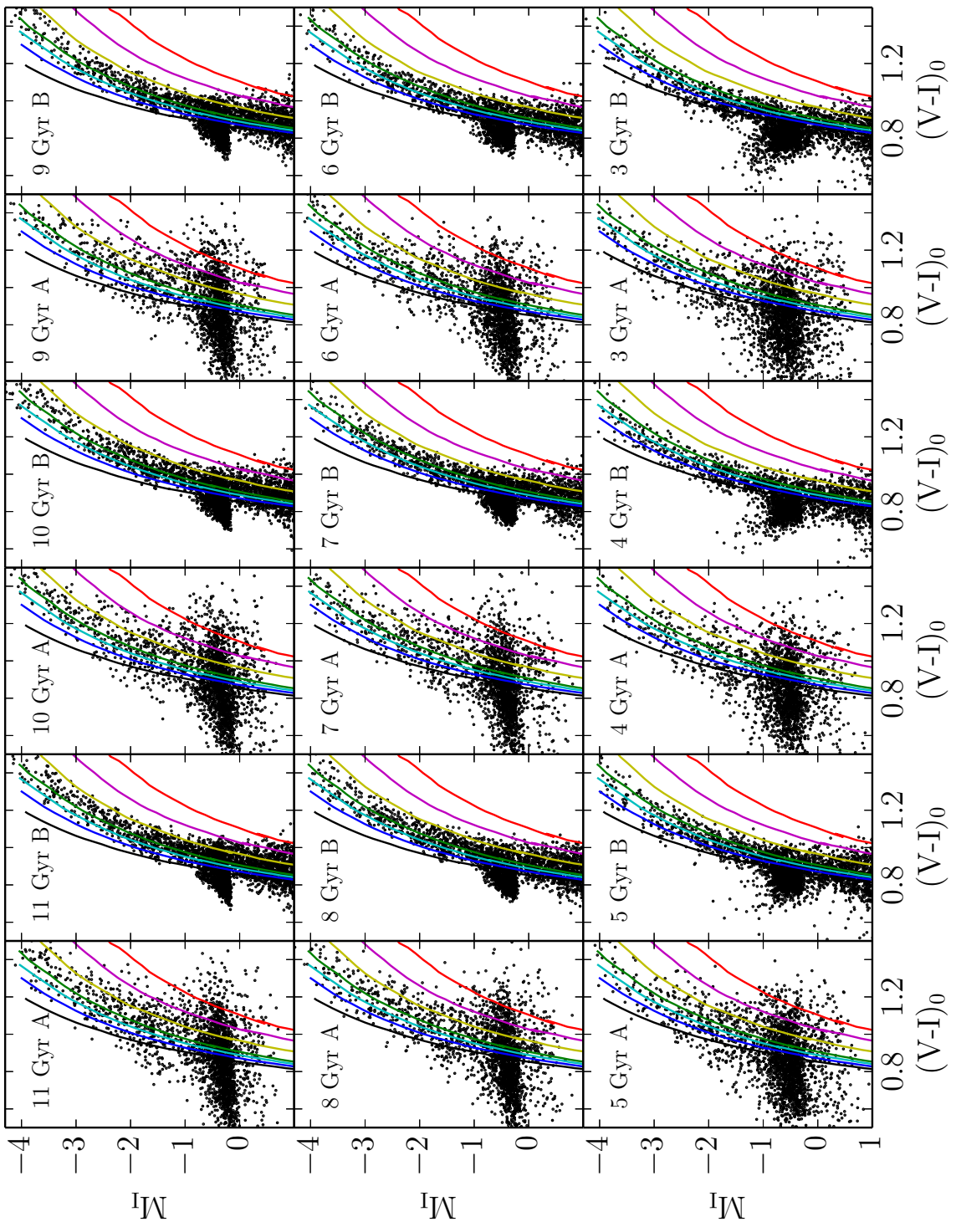

Fig. 7.— The model CMDs used in investigating the effects of an age error on a metallicity interpolation.

old population ($\gtrsim$10 Gyr) the RGB is relatively insensitive to the exact age. However, for younger populations this does not hold. To explore this further, we generated a series of synthetic CMDs each with the same properties as P4, except changing the mean age of the stars by 1 Gyr from 11 Gyr down to 3 Gyr. We then applied the observational profiles and interpolated in metallicity on the 12 Gyr isochrone grid to observe how the peak metallicity varies with a fixed adopted age of 12 Gyr. Each of these model CMDs is displayed in Figure 7.

Figure 8 shows how the metallicity discrepancy changes as a function of mean population age for model CMDs using the observational profiles A (circles) and B (triangles). Here, Δ[M/H] is in the sense $[M/H]_{out}$ -$[M/H]_{in}$. Figure 8 shows a clear trend in which populations younger than the isochrones in the model grid produce systematically more metal-poor metallicities. In accordance with previous studies, this effect is small ($\lesssim$0.1 dex) in populations older than 10 Gyr but may produce an error of nearly half a dex for considerably younger populations. Linear fits to the data resulted in the parameters presented in Table 3. The relations are incompatible with each other considering the quoted uncertainties. It seems that CMDs with smaller photometric errors along the RGB are more sensitive to age differences in their interpolated MDFs. Part of the decreased sensitivity for profile A may be the coupling between the isochrone grid and larger photometric errors discussed in Section 3.1.

Of particular note for the small error profile (*triangles*) is the discontinuous jump in metallicity error from 6 to 5 Gyr. It seems that this age range defines where the stars present on the interpolation grid become increasingly dependent on the age of the system.

On the other hand, for the case with larger errors (*circles*) we observe systematically more accurate peak metallicities. While this is certainly counter-intuitive, this is almost certainly a result of the coupling between the photometric errors and the adopted isochrone grid. As discussed in Section 3.1, the large photometric errors in profile A couple with the asymmetry of the isochrone grid to scatter more stars off of the metal-poor end compared with the metal-rich end of the grid. Thus, the seemingly more accurate

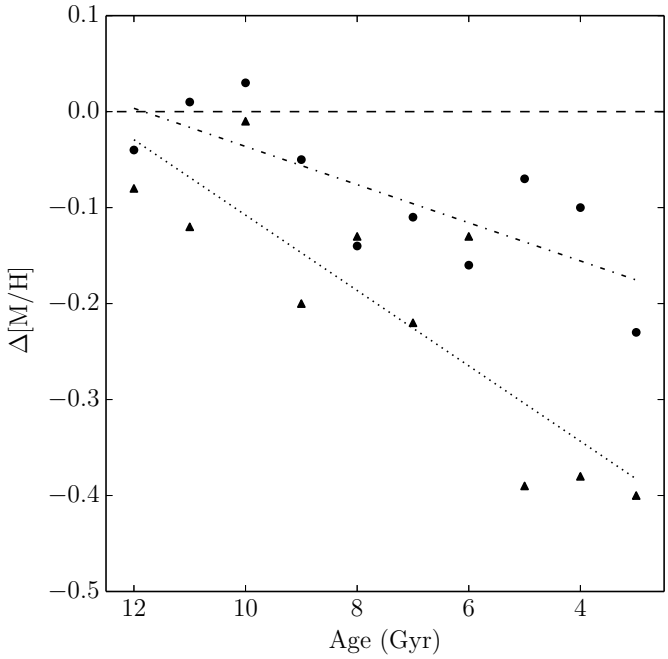

Fig. 8.— Peak metallicity discrepancy as a function of the mean age of a synthetic CMD. Circles represent CMDs modeled with observational profile A, while triangles are CMDs modeled with profile B. The dashed-dot and dotted lines show the linear fits for the two profiles A and B, respectively.

TABLE 3
LINEAR FIT PARAMETERS FOR METALLICITY ERROR VERSUS AGE OFFSET EXPERIMENTS.

Profile	Slope[a] (dex/Gyr)	Zero-point[a] (dex)	RMS scatter (dex)
A	0.020±0.007	-0.235±0.055	0.049
B	0.039±0.010	-0.501±0.079	0.069

[a]Quoted uncertainties represent the square roots of the diagonal elements from the covariance matrix returned from the fitting routine.

values for CMDs obtained applying profile A is more likely an artifact of the interpolation procedure rather than a reflection of the true accuracy.

3.6. Multiple Gaussian bursts: P5

We tested the effects of multiple epochs of star formation in a system by simulating a stellar population with 3 distinct star formation episodes. We achieved this by inputting a SFH into IAC-STAR which consisted of three Gaussian bursts of star formation at ages of 12, 8, and 4 Gyr. All have 1σ widths of 1 Gyr, and the AMR is monotonically increasing between the peaks of star formation. Both the SFH and AMR for this population, which we call P5, are illustrated in Figure 9. Applying the observational profiles and interpolating on the same isochrones as in previous sections yields CMDs 5A and 5B. These CMDs and corresponding interpolated MDFs are illustrated in Figure 10.

The peak of the input metallicity lies at [M/H] = -0.98 dex. Since the most recent star formation episode at 4 Gyr dominates the number of stars currently present on the RGB, the MDF is peaked at this metal-rich end. However, the interpolated MDFs for both CMDs 5A and 5B are significantly more metal-poor than this with peaks at [M/H]= $-1.18^{+0.07}_{-0.04}$ dex and [M/H]= $-1.22^{+0.22}_{-0.04}$ dex, respectively. It therefore seems that the most recent episode of star formation is being mistaken for a more-metal poor population owing to the old isochrone grid being used. This is in accordance with the results presented in Section 3.5, where we showed that for systems younger than ∼6 Gyr, the shape of the RGB becomes heavily dependent on the age, and relatively large errors in the peak metallicity are expected.

It is interesting to note that in the case of the smaller error profile (CMD 5B, Figure 10; lower right), two distinct peaks in the MDF are recovered through the interpolation. These peaks correspond roughly to the metallicity of the system during the peaks of the first two episodes of star formation ([M/H]∼-1.5 dex, 12 Gyr burst; [M/H]∼-1.3 dex, 8 Gyr burst; see Figure 9). These peaks are well-recovered in the interpolated MDF, highlighting the high fidelity of the RGB for metallicity estimates of old stars. On the other hand, the metallicity of the system during the youngest starburst ([M/H]∼ -1 dex, 4 Gyr; see Figure 9) completely lacks a peak in the interpolated MDF, further illustrating the ineffectiveness of the RGB metallicity estimation technique for stellar populations younger than 6 Gyr absent of an accurate age estimate.

3.7. The Effects of a Recent Star Formation Episode

We now turn to investigating the effect of a young starburst in more detail. To accomplish this, we synthesized a series of stellar populations each with two Gaussian star bursts, one at 12 Gyr, another at 4 Gyr, and both with 1σ widths of 1 Gyr. In each case of this series, the intensity of the young star formation episode was scaled down by a multiplicative factor such that its intensity ranged in 0.25-1.0 times the intensity of the old star burst. The AMR for all populations in this series are identical to P5. The same procedures for applying the observational profiles and performing the metallicity interpolation were then performed for each of these CMDs. Figure 11 shows the error in the peak metallicity of the interpolated MDF as a function of young starburst intensity.

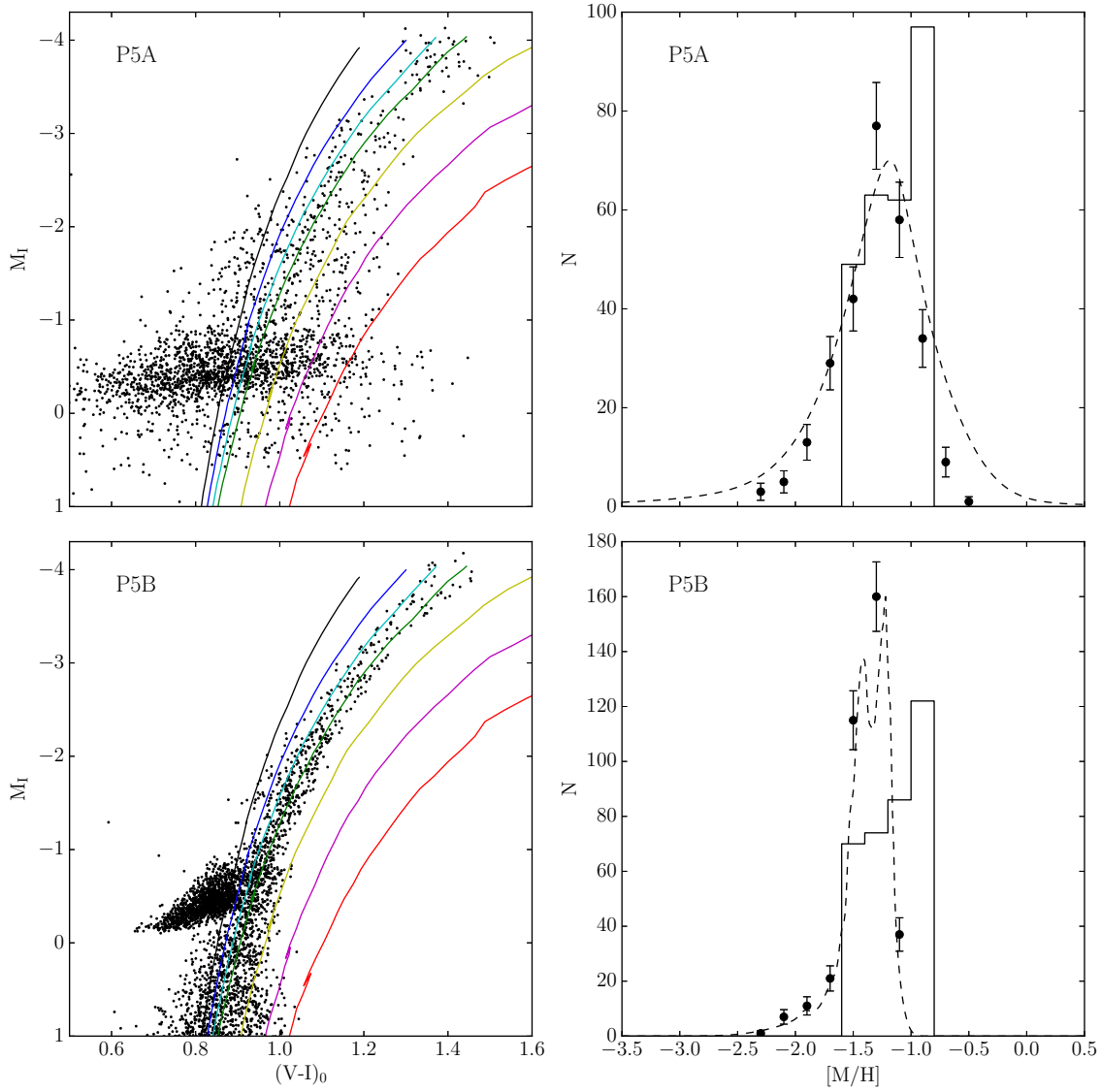

Fig. 10.— *Left:* The M_I, $(V\text{-}I)_0$ CMD for models 5A (*top*) and 5B (*bottom*). The model grid using the isochrones of Girardi et al. (2002) for an age of 12 Gyr and metallicities of $Z = 0.0001$, 0.0003, 0.0006, 0.001, 0.002, 0.004, and 0.008 are overplotted for reference.*Right:* The interpolated binned (points) and Gaussian smoothed (dashed line) MDFs for each corresponding model CMD. The error bars in the binned MDFs are 1σ Poisson uncertainties. The solid bar plots represent the input MDFs.

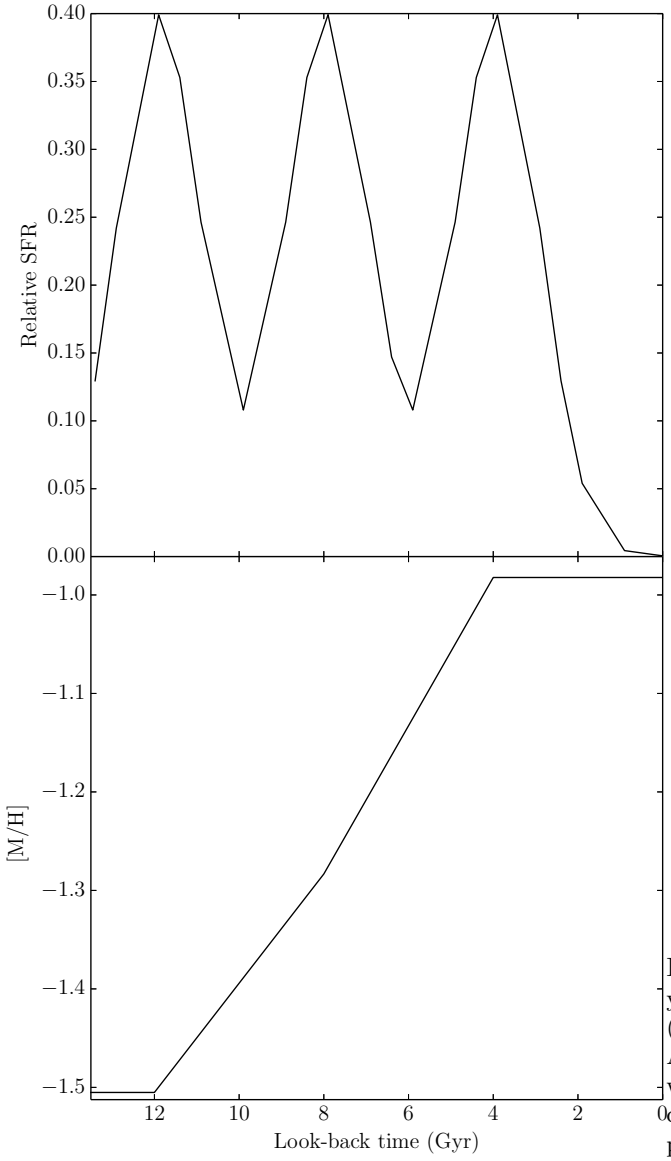

Fig. 9.— *Top:* The input SFH for P5 consisting of 3 Gaussian bursts of star formation. Note that IAC-STAR cannot take more than 20 nodes in time for the input SFH, hence the coarse resolution here. IAC-STAR does however interpolate amongst these nodes in time to achieve greater time resolution. *Bottom:* The input AMR for P5.

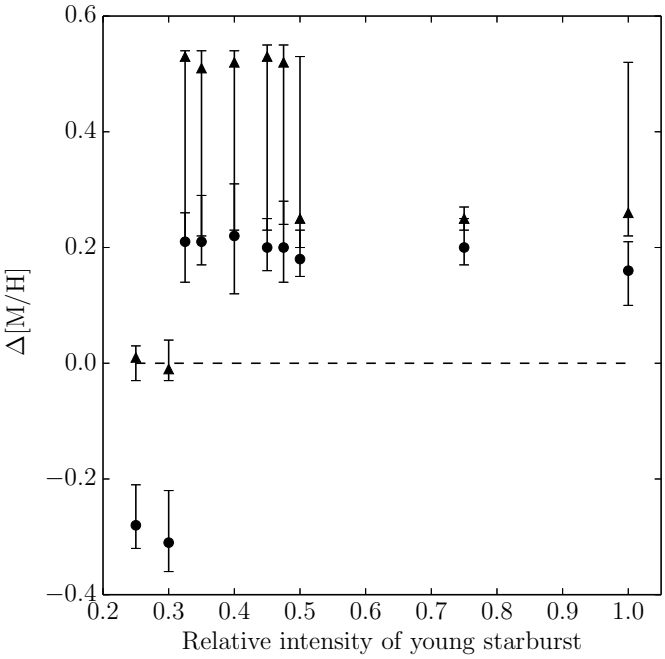

Fig. 11.— Peak metallicity error versus intensity of a young starburst (4 Gyr) relative to the old star burst (12 Gyr). CMDs produced with observational profile A are circles, while the triangles show CMDs produced with observational profile B. Error bars represent 99% confidence intervals returned from bootstrapping the peak of the interpolated MDF.

Inspection of Figure 11 reveals that for young starbursts $\lesssim$0.3 as strong as the old star burst, the peak of the MDF is well-recovered by interpolating on a grid of old isochrones. Once this young burst exceeds this threshold intensity, the young stars begin to dominate the MDF and the peak interpolated metallicity is in significant error when compared to the peak of the true MDF. Taking these results with those of the previous subsection, we conclude that a metallicity determination from the RGB of a stellar population that has experienced star formation within the last $\sim$6 Gyr that was at least 30% as intense as star formation in older epochs will produce a metallicities which are systematically in error by up to 0.5 dex.

3.8. The Effects of Binary Stars

Another component of stellar systems that may act to alter an interpolated MDF is binarity. Studies of the SFH of dwarf galaxies in the Local Group typically take the binary fraction as a free parameter in their analysis, and they report values around 40-60% (Hidalgo et al. 2009; Monelli et al. 2010; Hidalgo et al. 2011). We choose to test the affects of binary systems on the metallicity interpolation by introducing a binary population to P1. This population contains binary stars in 40% of the systems with a minimum mass ratio of $q = 0.5$, with the mass of the secondary chosen from a flat mass distribution. Subsequent interpolation as with the other synthetic CMDs did not reveal noticeably different MDFs from P1, forcing us to conclude that stellar populations with binary characteristics similar to those used here should not significantly affect a metallicity interpolation on the RGB.

4. Conclusions

We have explored a variety of different stellar population effects on the MDF constructed from the RGB stars in synthetic CMDs. In particular, we examine how realistic photometric error and completeness effects coupled with a variety of SFHs and AMRs alter the metallicities derived from an interpolation in M_I, $(V\text{-}I)_0$, and Z on the RGB. We summarize our findings for a variety of simulated model CMDs as follows:

1. For an old, simple stellar population, the RGB proves to be a very reliable metallicity indicator. In the worst case, peak metallicity values are recovered within less than 0.1 dex for photometry with errors that are relatively large compared with the extent of the isochrone grid. In the best case, peak metallicities are recovered to within 0.01 dex for more precise photometry. We determine the optimal magnitude range of RGB stars over which a metallicity interpolation should be performed to be restricted to stars between the RGB tip and $M_I = -1.5$ mag for the range of the photometric errors used in this exploration. Inherent spreads in the stellar metallicities and ages do not have significant effects on the modular interpolated metallicity.

2. It should be noted that the adopted isochrone grid can introduce significant systematic effects in the resultant MDF. Significant selection biases may present themselves in the subsequent interpolated MDF resulting from asymmetric scattering of the stars off of the model grid.

3. A stellar population significantly younger than 10 Gyr will yield systematically more metal-poor metallicities assuming an old age for the interpolating isochrones. The resulting discrepancy in peak metallicity as a function of age can be described with a linear relation. The slope of this relationship depends on the photometric error profile of the CMD, indicating that more precise photometry is more sensitive to this age error than photometry with larger errors. Thus, care should be taken to obtain an accurate age estimate when estimating metallicities from the RGB using precise photometry, especially if a significant possibility exists that the population is younger than 10 Gyr.

4. Using a grid of old isochrones, a star formation episode occurring less than $\sim$6 Gyr ago produces a significant, systematic error in the interpolated MDF. This can result in metallicities that are erroneously poor by up to 0.5 dex. Along the same vein, if a recent starburst is $\gtrsim$30% as intense as older star formation events with comparable durations in time, the interpolated MDF will yield a significantly erroneous peak.

We close by noting that the RGB of old stellar populations has proven itself as a reliable metallicity estimator in our study. For reasonably simple SFHs, the RGB provides a very accurate estimate of the average metallicity of a stellar population. However, if the system in question has experienced any significant star formation within the past few Gyr, metallicities derived from the RGB may be in error by up to 0.5 dex. Therefore, when applied to stellar systems with potentially complex stellar populations, more care needs to be taken if using the RGB to estimate the metallicity of the system. In particular, a reasonably accurate estimate of the age of the system should be obtained through an independent, reliable estimator. Additionally, one should be reasonably certain that no significant star formation has occurred within the past few Gyr in the system in question, otherwise there is a high risk of significant systematic errors in the derived metallicities.

We would like to thank Aaron Grocholski for helping to write the original IDL interpolation code modified for use in this work, as well as for his comments on an earlier draft of this paper. We are also grateful to Mike Barker and Sebastian Hidalgo for their insightful comments and suggestions on an early draft of this paper. Finally, we thank the anonymous referee who provided helpful comments to increase the clarity of the paper. This work has made use of the IAC-STAR Synthetic CMD computation code. IAC-STAR is supported and maintained by the computer division of the Instituto de Astrofsica de Canarias.

REFERENCES

Aparicio, A. & Gallart, C., 2004, AJ, 128, 1465

Barker, M. K., Sarajedini, A., & Harris, J., 2004, ApJ, 606, 869

Chiosi, C., 1998, in *Stellar Astrophysics for the Local Group*, VIII Canary Islands Winter School of Astrophysics, eds. Aparicio, A., Herrero, A., & Sánchez, F., Cambridge University Press.

Da Costa, G. S. & Armandroff, T. E., 1990, AJ, 100, 162

Durrell, P. R., Harris, W. E., & Pritchet, C. J., 2001, AJ, 121, 2557

Girardi, L., Bressan, A., Bertelli, G., & Chiosi, C. 2000, A&AS, 141, 371

Girardi, L. et al., 2002, A&A, 391, 195

Hidalgo, S. L., Aparicio, A., Martínez-Delgado, D., & Gallart, C., 2009, ApJ, 705, 704

Hidalgo, S. L. et al., 2011, ApJ, 730, 14

Kroupa, P., 2001, MNRAS, 322, 231

McConnachie, A., Arimoto, N., Irwin, M., & Tolstoy, E., 2006, MNRAS, 373, 715

Monelli, M., 2010, ApJ, 720, 1225

Salaris, M. & Girardi, L., 2005, MNRAS, 357, 669

Sarajedini, A. et al., 2002, ApJ, 567, 915

Sarajedini, A. & Jablonka, P., 2005, AJ, 130, 1627

Saviane, I., Rosenberg, A., Piotto, G., & Aparicio, A., 2000, A&A, 355, 966

Streich, D., de Jong, R. S., Bailin, J., Goudfrooij, P., Radburn-Smith, D., & Vlajic, M., 2014, A&A, 563, A5